Annals of Biomedical Engineering, Vol. 44, No. 8, August 2016 (© *2016*) pp. 2402–2416
DOI: 10.1007/s10439-015-1545-7

Long-Term Functional Efficacy of a Novel Electrospun Poly(Glycerol Sebacate)-Based Arterial Graft in Mice

RAMAK KHOSRAVI,[1] CAMERON A. BEST,[2] ROBERT A. ALLEN,[3] CHELSEA E. T. STOWELL,[3] EKENE ONWUKA,[2] JENNIFER J. ZHUANG,[3] YONG-UNG LEE,[2] TAI YI,[2] MATTHEW R. BERSI,[1] TOSHIHARU SHINOKA,[2] JAY D. HUMPHREY,[1] YADONG WANG,[3] and CHRISTOPHER K. BREUER[2]

[1]Department of Biomedical Engineering, Yale University, 55 Prospect Street, New Haven, CT 06511, USA; [2]Tissue Engineering Program and Surgical Research, Nationwide Children's Hospital, 575 Children's Crossroads, Research III – WB4151, Columbus, OH 43215, USA; and [3]Department of Bioengineering, University of Pittsburgh, 3700 O'Hara Street, Pittsburgh, PA 15261, USA

(*Received 31 August 2015; accepted 22 December 2015; published online 21 January 2016*)

Associate Editor Ender Finol oversaw the review of this article.

Abstract—Many surgical interventions for cardiovascular disease are limited by the availability of autologous vessels or suboptimal performance of prosthetic materials. Tissue engineered vascular grafts show significant promise, but have yet to achieve clinical efficacy in small caliber (<5 mm) arterial applications. We previously designed cell-free elastomeric grafts containing solvent casted, particulate leached poly(glycerol sebacate) (PGS) that degraded rapidly and promoted neoartery development in a rat model over 3 months. Building on this success but motivated by the need to improve fabrication scale-up potential, we developed a novel method for electrospinning smaller grafts composed of a PGS microfibrous core enveloped by a thin poly(ε-caprolactone) (PCL) outer sheath. Electrospun PGS–PCL composites were implanted as infrarenal aortic interposition grafts in mice and remained patent up to the 12 month endpoint without thrombosis or stenosis. Many grafts experienced a progressive luminal enlargement up to 6 months, however, due largely to degradation of PGS without interstitial replacement by neotissue. Lack of rupture over 12 months confirmed sufficient long-term strength, due primarily to the persistent PCL sheath. Immunohistochemistry further revealed organized contractile smooth muscle cells and neotissue in the inner region of the graft, but a macrophage-driven inflammatory response to the residual polymer in the outer region of the graft that persisted up to 12 months. Overall, the improved surgical handling, long-term functional efficacy, and strength of this new graft strategy are promising, and straightforward modifications of the PGS core should hasten cellular infiltration and associated neotissue development and thereby lead to improved small vessel replacements.

Keywords—Elastomer, Neoartery development, Electrospinning, Cell-free polymeric scaffold, Murine model.

ABBREVIATIONS

TEVG	Tissue engineered vascular graft
PGS	Poly(glycerol sebacate)
PCL	Poly(ε-caprolactone)
SCPL	Solvent casted particulate leached
IAA	Infrarenal abdominal aorta

INTRODUCTION

Over 600000 patients per year in the United States require vascular grafts for different reasons, including vascular bypass, hemodialysis, and repair of congenital heart defects.[2] Clinically available synthetic vascular grafts lack growth potential and are prone to serious complications—including stenosis, thrombosis, and infection—that necessitate revision procedures.[1] These complications result primarily from the long-term presence of synthetic (nonliving) biomaterials.[24] To overcome limitations of permanent synthetic grafts, many research groups have developed autologous blood vessels through tissue engineering. A common approach is to grow a living vessel *ex vivo*,[5,18,30] but this carries limitations such as high production costs and long lead times.[24] To reduce costs and enable off-the-shelf avail-

---

Address correspondence to Ramak Khosravi, Department of Biomedical Engineering, Yale University, 55 Prospect Street, New Haven, CT 06511, USA. Electronic mail: ramak.khosravi@yale.edu, christopher.breuer@nationwidechildrens.org

Ramak Khosravi, Cameron A. Best, Robert A. Allen, and Chelsea E.T. Stowell have contributed equally to this work.

ability, we and others have employed scaffold-based strategies in which a seeded or cell-free resorbable scaffold is implanted directly in a patient.[11] These tissue engineered vascular grafts (TEVGs) harness the body's regenerative potential to form a new blood vessel *in vivo*.

We previously demonstrated that cell-free resorbable TEVGs can remodel rapidly into neoarteries in an *in vivo* rat model.[29] These grafts consisted of an inner layer of solvent casted, particulate leached (SCPL) poly(glycerol sebacate) (PGS) to promote host cell infiltration and rapid remodeling, and an outer layer of poly(ε-caprolactone) (PCL) for mechanical support. Although the surgical handling and production yield of these SCPL grafts were adequate, switching to a fibrous graft design could greatly accelerate manufacturing scale-up and clinical adoption. Thus, we developed a new method for electrospinning PGS microfibers. Compared with SCPL fabrication, electrospinning improves suture retention, ultimate tensile strength, and strain to failure while also improving fabrication throughput and reproducibility.[12]

In this paper, we present the first long-term, longitudinal study of the *in vivo* functional efficacy of these new TEVGs in mice. A major advantage of murine models is that they allow extensive characterization of molecular and cellular mechanisms underlying graft remodeling and vascular neotissue formation over long periods.[23] Despite the presence of residual polymer up to 12 months, the present data revealed many favorable outcomes, including no graft-related mortality, no catastrophic graft failures, no thrombosis or stenosis in the absence of anti-platelet therapy and anti-coagulation, cellular infiltration into the PGS core with, most notably, differentiated contractile smooth muscle cells in the "medial" layer, substantial fibrillar collagen accumulation, and remodeling of both the graft and the adjacent aorta. Yet, the microfibrous PGS core had a reduced porosity and pore size when compared with the SCPL PGS core, which likely delayed the rapid cellular infiltration and early interstitial remodeling observed previously and contributed to a progressive luminal enlargement of the TEVG over the first 6 months. Hence, the new design and fabrication strategy revealed both a favorable long-term outcome and important insight into ways to improve key scaffold physical parameters to yield the next generation of electrospun PGS vascular grafts.

MATERIALS AND METHODS

Graft Fabrication

We fabricated grafts by compositing two tubular layers: a thicker inner layer (PGS) that yielded a resorbable elastomeric "core" and a thinner outer layer (PCL) that provided a stiffer, longer-lasting "sheath". The PGS prepolymer (pPGS) was synthesized in house as previously described.[28] Other materials included poly(vinyl alcohol) (PVA) (Soarus LLC, Arlington Heights, IL), 1,1,1,3,3,3-hexafluoroisopropanol (HFIP) (Oakwood Products Inc., West Columbia, SC), hyaluronic acid sodium salt (Sigma-Aldrich, St. Louis, MO), PCL (M_n 80 kDa) (Sigma-Aldrich), and 2,2,2-trifluoroethanol (TFE) (Acros Organics, Belgium).

We first constructed tubes of PGS microfibers by (1) electrospinning pPGS-PVA blends, (2) thermally crosslinking the pPGS to form PGS, and (3) purifying with water and ethanol to remove the majority of the PVA (Figs. 1a-1 and 1a-2; techniques modified from[12]). Briefly, an electrospinning solution was prepared by mixing pPGS and PVA at a 55:45 mass ratio and dissolving at 16% w/v in HFIP overnight. To form pPGS–PVA microfibers, the solution was pumped at 29 μL/min through a 22 gauge needle that served as the spinneret. Positive and negative 12 kV were applied, respectively, to the spinneret and another needle that served as the anode. pPGS–PVA microfibers initially deposited onto a 9 mm diameter plastic rod held at an elevated position between the spinneret and the anode were subsequently drawn onto a hyaluronic acid-coated 0.78 mm diameter stainless steel mandrel. The anode was positioned 55 cm from the spinneret; the mandrel was placed between the two, at 30 cm from the spinneret, and rotated at 100 or 300 RPM, alternating every 100 μL of solution spun to collect a combination of loosely-wound and tightly-wound fibers. Depending on fiber collection efficiency, 1.15–1.25 mL of solution was dispensed.

To crosslink the pPGS into PGS, fiber-coated mandrels were heated under vacuum (−60 mm Hg) at 120 °C for 24 h, then at 150 °C for an additional 24 h. Electrospun microfibrous PGS cores were purified and isolated as follows: (1) To remove PVA, the fiber-coated mandrels were washed using 3 changes of deionized water, followed by a fourth wash overnight with agitation. The washes with deionized water also dissolved the hyaluronic acid coating from the mandrels, thus allowing the microfiber tube to be isolated easily from the mandrel. (2) To remove unreacted monomers and oligomers, electrospun microfibrous PGS cores were washed in a graded series of ethanol solutions, then left in 100% ethanol overnight. The washes were performed again in reverse order to remove residual ethanol, ending with overnight washing in DI H_2O. Individual 5 mm graft cores of ~220 μm wall thickness were cut from the length of core. We next affixed PCL sheaths to the PGS cores as previously described,[29] with some modification (Figs. 1a, 2, and 3). To improve the resistance of the PGS core to

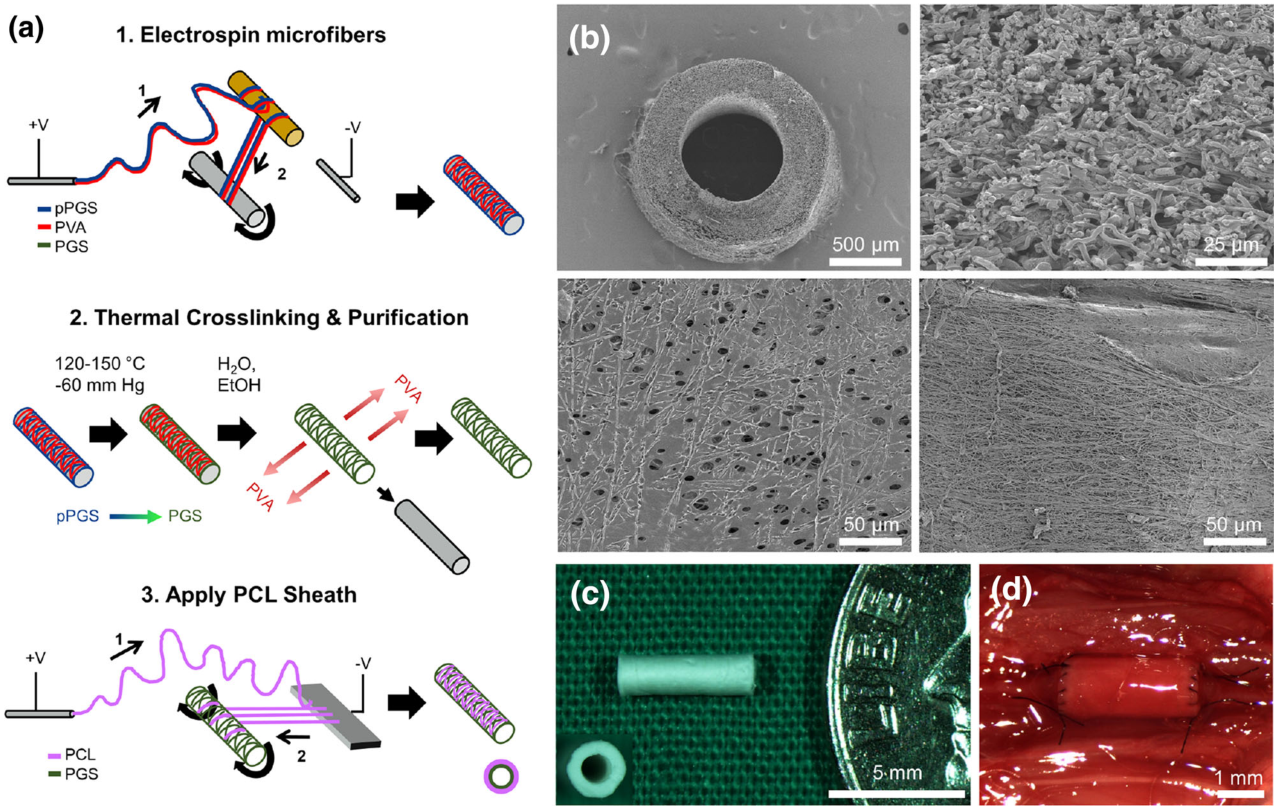

FIGURE 1. TEVG fabrication and structure. A. Schema of the fabrication process. *A1—Electrospin microfibers*. A polymer solution containing pPGS (blue) and PVA (red) is infused through a positively charged spinneret to form a polymer jet that deposits onto a plastic rod (1) and then is drawn onto a rotating stainless steel mandrel (2). The result is a mandrel coated with microfibers of a pPGS-PVA blend (right). *A2—Thermal Crosslinking and Purification*. Microfiber coated mandrels are thermally crosslinked to convert pPGS (blue) into PGS (green). PGS-PVA microfibers are then purified in water and ethanol to remove the PVA, which yields a microfibrous tubular core composed primarily of PGS (right). *A3—Apply PCL Sheath*. A PCL solution (purple) is infused through a positively charged spinneret to form a polymer jet that initially deposits onto an aluminum plate anode (1) and then is drawn onto the rotating PGS core (2). The result (right) is a composite graft consisting of an electrospun PGS microfiber core (green) and an electrospun PCL fiber sheath (purple). B. Graft microstructure visualized by Scanning Electron Microscopy. Top left—Transverse cross-section at 50×. Top right—Transverse cross-section of the electrospun PGS core at 1000× shows a network of microfibers with space between some fibers and limited fusion between others. Bottom left—Luminal surface of graft at 400× magnification. Fused fibers create a smooth surface in some regions, but frequent gaps in fusion provide access to the space within the PGS core. Bottom right—Abluminal view of the graft at 400× magnification shows coverage with the PCL sheath, consisting of microfibers and nanofibers. C. Macroscopic view of a finished graft prior to implantation; the graft is pictured next to an American dime for size comparison. Inset—transverse view of finished graft. D. *In situ* view of a TEVG conducting blood flow on the day of implantation.

compression during sheath application, the cores were hardened by freeze-drying in a 30% w/v NaCl solution using a lyophilizer; this process effectively filled the pores with NaCl crystals. Hardened PGS cores were mounted on uncoated stainless steel mandrels (0.78 mm inner diameter) for PCL sheath application. The PCL electrospinning solution was prepared by dissolving PCL at 14% w/v in a 5:1 solution of TFE:H_2O. To form PCL fibers, the PCL solution was pumped at 29 μL/min through a 22 gauge needle serving as the spinneret. Positive and negative 12 kV were applied, respectively, to the spinneret and a 6 cm × 4 cm aluminum plate serving as the anode. PCL fibers initially collected onto the aluminum plate placed 25 cm from the spinneret, but were subsequently drawn onto the hardened PGS core template held 2–3 cm from the plate and rotated at 50 RPM. Fiber collection continued until sheath thickness reached approximately 10 μm.

The resultant PGS–PCL composite grafts were purified of NaCl by washing in 3 changes of DI H_2O, then freeze-dried and stored in desiccant at room temperature. Grafts used for implantation were sterilized with ethylene oxide (12 h cycle in an Anprolene AN74i gas sterilizer, Anderson Sterilizers Inc., Burlington, NC). Residual ethylene oxide was removed with 24 h of additional aeration and washing overnight in sterile PBS prior to implantation.

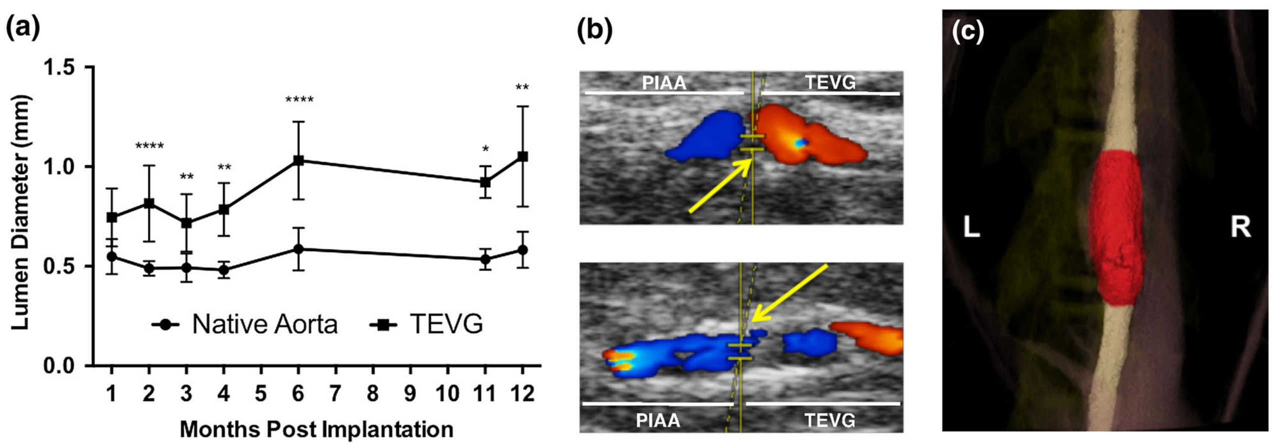

FIGURE 2. (A) Serial ultrasound assessment of implanted electrospun TEVGs and adjacent abdominal aorta. Values are a mean ± SD of averages of at least 3 measurements of the TEVG and adjacent aorta per animal per time point. $*p < 0.05$, $**p < 0.005$, $****p < 0.00005$. (B) Representative doppler ultrasound images of grafts with dilation (top) and no dilatation (bottom) 12 months post-implantation; yellow arrows indicate the proximal anastomosis, with the adjacent proximal infrarenal abdominal aorta (PIAA) on the left and the implanted electrospun TEVG on the right. (C) 3-D reconstruction of μCT imaging of graft at 12 months post-implantation. The graft is highlighted in red, and the adjacent proximal and distal abdominal aorta is colored white.

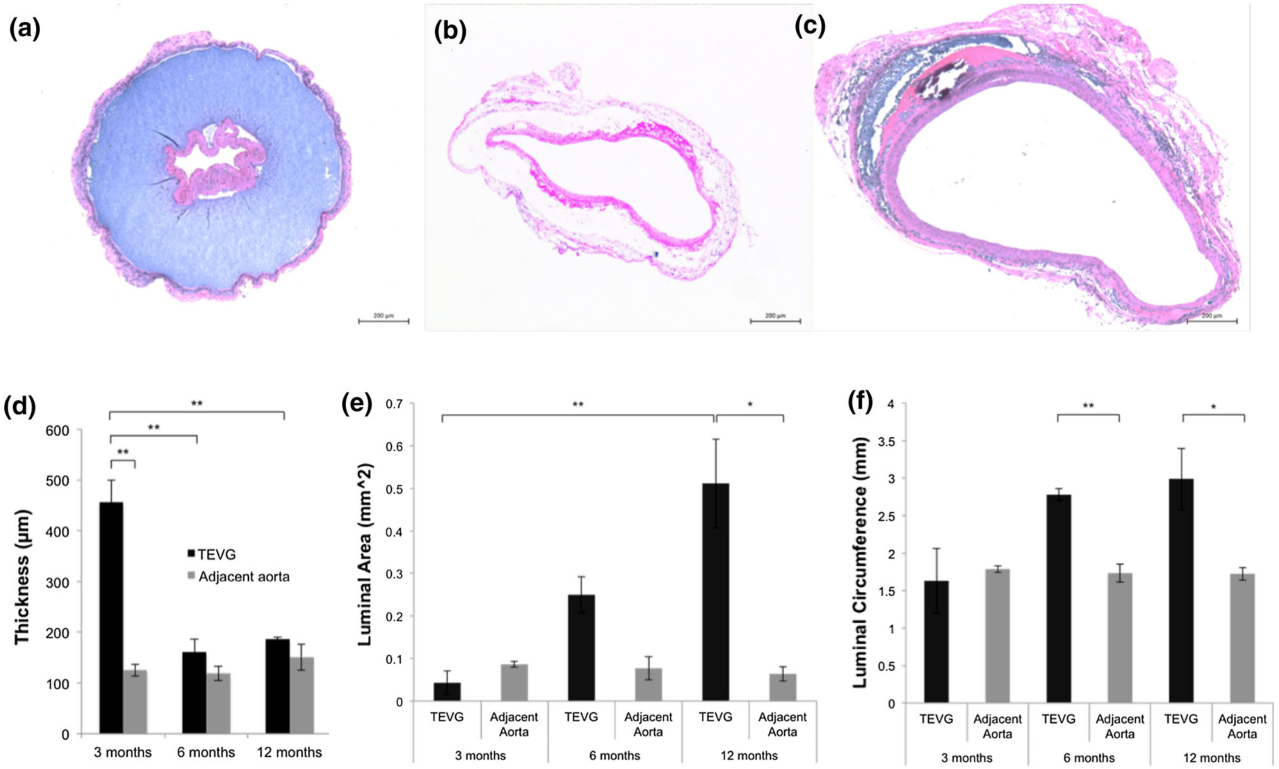
(a)
(b)
(c)
200 µm
200 µm
200 µm
(d)
Thickness (µm)
0
100
200
300
400
500
600
**
**
**
TEVG
Adjacent aorta
3 months
6 months
12 months
(e)
Luminal Area (mm^2)
0
0.1
0.2
0.3
0.4
0.5
0.6
0.7
**
*
TEVG
Adjacent Aorta
3 months
6 months
12 months
(f)
Luminal Circumference (mm)
0
0.5
1
1.5
2
2.5
3
3.5
4
**
*
TEVG
Adjacent Aorta
3 months
6 months
12 months

FIGURE 3. H&E staining of TEVGs retrieved at 3 months (A), 6 months (B), and 12 months (C) after implantation. (D) Quantification of electrospun graft wall thickness. Graft luminal expansion was confirmed by quantification of luminal area (E) and luminal circumference (F) from histological images. Values are mean ± SEM. $*p < 0.05$, $**p < 0.005$.

Physical Characterization of the Grafts

The porosity ϕ of the PGS core was measured gravimetrically according to,

$$\phi = 1 - \frac{\rho_{\text{bulk}}}{\rho_{\text{matl}}} \qquad (1)$$

where ρ_{bulk} represents the bulk mass density of the PGS core and ρ_{matl} the mass density of nonporous PGS. The latter is reported to be 1.1 g/cm^3 whereas the former was calculated by dividing the mass of the PGS core by its volume while constrained by the sheath.[20]

PGS core mass and volume were determined by finding the mass and volume of the composite graft and subtracting the estimated mass and volume of the PCL sheath. Inner and outer diameters of the PCL sheath were measured on transverse graft sections viewed by scanning electron microscopy (SEM) and analyzed with ImageJ software (NIH, Bethesda, MD). The calculated PCL volume was used to approximate the mass of PCL using the manufacturer's reported density, 1.21 g/cm^3 and the assumption of a nonporous sheath.

Pore size and fiber diameter were measured from SEM images of cross-sections of the grafts using ImageJ. Pore size and fiber diameter were sampled along a representative radial line drawn on four SEM fields per graft (400× magnification for pore size, 1000× for fiber diameter), then data were pooled for all three measured grafts. Pore area was estimated by treating each pore as an ellipse, thus calculating area from the conjugate diameters and reporting the effective diameter (i.e., diameter of a circular pore having the same area).

Accelerated hydrolytic degradation of PGS cores was measured *in vitro* by mass loss under basic conditions. To produce 3-mm diameter PGS disks, electrospun microfibrous PGS cores were slit along the long axis, stretched flat, and then cut with a 3 mm diameter hole punch. For comparison, we also tested SCPL PGS cores that were fabricated as previously described[29] and similarly cut into disks. Dry weight was recorded for each disk, which was then placed in 1.5 mL Eppendorf tubes containing 1 mL of 34 mM bicarbonate buffer adjusted to pH 11.75 with NaOH. Eppendorf tubes were incubated on a heated rocking plate set to 37 °C. Disks were retrieved at 12, 24, and 36 h and rinsed 3× with deionized water, then freeze-dried and weighed to determine final dry weight.

Animal Care and Use

All animals received humane care in compliance with the National Institutes of Health (NIH) Guide for the Care and Use of Laboratory Animals. The Institutional Animal Care and Use Committee of The Research Institute at Nationwide Children's Hospital approved and monitored the use of animals and all animal procedures. Grafts were implanted in nine ($n = 9$) female C57BL/6 mice at 8 to 12 weeks of age (Jackson Laboratories, Bar Harbor, ME, USA) and harvested after 3, 6, or 12 months ($n = 3$ per time point).

Specifically, microfiber PGS–PCL scaffolds were implanted as infrarenal aortic interposition grafts using standard aseptic microsurgical technique as previously described.[14] Briefly, mice received an intraperitoneal injection of preanesthesia analgesic (ketoprofen, 10 mg/kg), then were anesthetized with ketamine (100 mg/kg) and xylazine (10 mg/kg). After achieving a surgical plane of anesthesia, the abdomen was opened *via* a midline incision, abdominal organs were eviscerated, and a 3.0 mm portion of the infrarenal abdominal aorta (IAA) was identified, isolated, cross-clamped, and divided. Scaffolds were then implanted as interposition grafts using running 10-0 nylon sutures to create end-to-end proximal and distal anastomoses. All animals received routine postoperative care without anti-coagulation and anti-platelet therapy.

Implanted grafts were monitored longitudinally until explant with high frequency ultrasonography (Vevo® 2100, VisualSonics Inc, Toronto, Canada). After induction of anesthesia (1.5% inhaled isoflurane vaporized with 100% O_2 at 1 L/min), the ventral abdomen was chemically depilated and ultrasound gel applied. Body temperature was maintained at 38 °C for the duration of ultrasound examination. At least 3 long axis images per TEVG and adjacent aorta were recorded, per animal per time, using either color Doppler or B-Mode ultrasound after confirmation of arterial flow with pulse wave Doppler. Quantification was achieved with ImageJ (NIH) for both the TEVG and the adjacent artery, with measurements for the TEVG including the distal anastomosis, proximal anastomosis, and mid-graft regions. In this way, four data points averaged over 3+ scans were generated per animal per time: a mean luminal diameter of the TEVG, proximal and distal anastomoses, and adjacent host artery. These data were averaged further over $n = 3$ mice to determine an overall mean luminal diameter ± SD at 0, 3, 6, and 12 months, hence yielding 12 data points per region for assessing longitudinal changes.

In addition, one graft was evaluated using contrast enhanced micro-computed tomography (μCT) 12 months after implantation. The mouse was anesthetized with an intraperitoneal injection of ketamine (300 mg/kg) and xylazine (30 mg/kg), a thoracotomy was performed, and the thoracic aorta was cannulated to administer a bolus injection of contrast (300 μL Omnipaque; Amersham Biosciences, Piscataway, NJ). μCT angiography was performed with the GE eXplore Locus μCT scanner (GE Healthcare, Milwaukee, WI).

At the appropriate endpoint, mice were euthanized by an intraperitoneal injection of ketamine (300 mg/kg) and xylazine (30 mg/kg), followed by induction of pneumothorax. Mice were then systemically perfused with cold 1× phosphate buffered saline (PBS). Just prior to explant, small sutures were placed at multiple locations along the graft, proximal IAA, and distal IAA, and photographs were taken to record suture positions *in situ* and *in vitro*, immediately following excision. Distances between these suture markers were determined using ImageJ and used to estimate *in vivo* axial stretches (the ratio between loaded and unloaded axial lengths of each segment). A continuous vascular segment, consisting of the graft plus a 1 to 2 mm portion of native IAA distal and proximal to the sites of anastomosis, was then harvested and placed in 1× Hank's Buffered Salt Solution (HBSS) until biaxial mechanical testing. To ensure adequate pressurization during mechanical testing, any included branches were identified and ligated.

Biaxial Mechanical Testing

The composite vessel (proximal IAA-TEVG-distal IAA) was cannulated and secured to custom drawn micropipettes with 6-0 suture. The cannulated vessels were placed in a custom computer-controlled biaxial testing device[10] within HBSS and initial dimensions were recorded in the unloaded state. Prior to testing, vessels were equilibrated at 80 mmHg with low intraluminal flow for 15 min at their estimated *in vivo* axial stretch, and subsequently preconditioned at this axial stretch *via* 4 cycles of pressurization from 10 to 140 mmHg. Following preconditioning, unloaded dimensions were measured again, and the *in vivo* axial stretch of the composite vessel was estimated *in vitro* by identifying the axial stretch at which the measured axial force remained nearly constant in response to changes in luminal pressure.[26] With the camera focused on the central region of the graft, all specimens were subjected to two cycles each of pressure-diameter testing consisting of cyclic pressurization from 10 to 140 mmHg at the experimentally determined *in vivo* axial stretch ratio (and at ±5% of this value). Pressure-diameter testing was then repeated with the camera focused on the proximal IAA. Luminal pressure, axial force, outer diameter, and overall axial length were measured continually throughout testing. Stress, stiffness, and the energy dissipation ratio (EDR) were quantified as previously described.[7]

Histology, Immunohistochemistry, and Immunofluorescence

Following mechanical testing, samples were fixed in 10% formalin at 4 °C for 24 h, dehydrated, paraffin embedded, and serially sectioned (4 μm thick sections). Representative sections were analyzed at 5 regions of interest: proximal IAA, proximal anastomosis, TEVG, distal anastomosis, and distal IAA. Histological analysis was based on five stains: hematoxylin and eosin (H&E), Masson's trichrome (TRI), Picrosirius Red (PSR), Hart's, and von Kossa (VK). Comparisons of aortic structure following testing with images obtained independently on samples from vessels that were not tested allow assessment of possible test-induced structural damage.

For immunohistochemical (IHC) analysis, slides were rehydrated and blocked for both endogenous peroxidase activity (0.3% H_2O_2 in MeOH) and nonspecific background staining (Background Sniper, BioCare Medical). Antigens were retrieved with citrate buffer and slides were incubated overnight at 4 °C with the following primary antibodies: rabbit anti-collagen I (1:250, Abcam), rabbit anti-collagen III (1:250, Abcam), anti-human smooth muscle actin (α-SMA, which cross reacts with mouse, 1:500, Dako), rabbit anti-calponin (1:200, Abcam), and rat anti-F4/80 (1:1000, AbD Serotec). Primary antibody binding was detected by incubation with species-appropriate biotinylated secondary antibodies (Vector) followed by binding of horseradish peroxidase streptavidin and subsequent chromogenic development with 3,3-diaminobenzidine (Vector). Finally, nuclei were counterstained with Gill's hematoxylin, and slides were dehydrated and cover-slipped. For immunofluorescence detection, sections were rehydrated and antigen retrieval performed as described above. Sections were then blocked for nonspecific binding (3% Normal Goat Serum) and incubated overnight at 4 °C with the following primary antibodies: rabbit anti-smooth muscle-myosin heavy chain (SM-MHC,1:1000, Abcam), anti-human α-SMA (1:500, Dako), rabbit anti-Cleaved Caspase-3 (1:500, Cell Signaling Technology), and rabbit anti-runt-related transcription factor 2 (RUNX-2,1:500, Abcam). Antibody binding was detected by subsequent incubation with a cocktail of goat anti-mouse Alexa-Fluor® 647 (1:300, Life technologies) and goat anti-rabbit Alexa-Fluor® 488 (1:300, Life Technologies) followed by nuclear counterstaining with DAPI (Life Technologies). Fluorescent images were acquired with a Ziess Axio Observer Z.1 microscope and a Zeiss Axiocam 503 digital camera.

Light field slides were imaged using an Olympus BX/51 microscope and associated Olympus DP70 digital camera, with PSR images taken under polarized light. Analysis of the digital images was performed using a custom MATLAB script that converts the original red, green, blue (RGB) images to the hue, saturation, lightness (HSL) color space to enable additional pixel-specific thresholding and delineation of individual constituents of interest, as previously described.[4] For PSR-stained sections, area fractions of red, orange, yellow, and green pixels were quantified to identify relative distributions of large and small collagen fibers as well as differences in fibrillar collagen packing at each time and throughout the 5 regions of interest. The RGB images were first inverted, then converted to the HSL color space, with HSL parameters chosen to isolate light blue pixels ($H = 160°–210°$,

TABLE 1. Physical properties of two PGS cores.

Parameter	Electrospun PGS microfibers	SCPL PGS foam[4]
Pore size (μm)	1.87 ± 0.23	21.2 ± 0.79
Porosity (%)	47.1 ± 4.2	81.1 ± 0.7
Fiber diameter (μm)	1.45 ± 0.06	N/A
Degradation rate (mass loss at pH 11.75) (%/h)	1.33	1.34
Young's modulus (MPa)	0.67–0.87[1]	0.243 ± 0.072

TABLE 2. TEVG geometry at implantation.

	Electrospun PGS–PCL composite	SCPL PGS–PCL composite[4]
Animal model	Mouse	Rat
Implantation site	Infrarenal abdominal aorta	Infrarenal abdominal aorta
Length (mm)	3–5	8–10
Inner diameter (μm)	718.9 ± 19.2	723 ± 1.33
Outer diameter (μm)	1164 ± 35.6	1313 ± 7.50
PGS core thickness (μm)	222.5 ± 21.1	236 ± 10.3
PCL sheath thickness (μm)	10.8 ± 2.88	15.7 ± 6.11

$S = 0.1$–1.0, $L = 0.47$–1.0). Associated area fractions were calculated based on the total number of pixels that satisfied the HSL threshold requirements for each constituent, divided by the total number of pixels identified as having any HSL parameter values other than those for the color black (the uniform background color).

RESULTS

Electrospinning (Fig. 1a) produced composite TEVGs comprised of a PGS core and PCL sheath (Fig. 1b). SEM showed further that the PGS cores consisted mainly of microfibers (~1.5 μm in diameter; Table 1), with space between some fibers and limited fusion of others (Fig. 1b, *top right*). The luminal surface of the PGS cores had some regions of superficial fiber fusion, but frequent gaps in fusion provided access to the space within the core wall (Fig. 1b, *bottom left*). The sheath consisted of micro- and nano-PCL fibers (Fig. 1b, *bottom right*), and accounted for $<5\%$ of the total graft thickness (Table 2).

These electrospun PGS–PCL grafts differed in physical properties and geometry from previously reported SCPL-based grafts.[29] Table 1 compares physical properties of the PGS cores for the two methods of fabrication. Electrospun PGS grafts had reduced porosity, reduced pore size, and a threefold higher bulk Young's Modulus compared with SCPL PGS grafts. Because the microfiber grafts were designed for interpositional implantation into a mouse, not rat, abdominal aorta, they were also implanted having a shorter length and reduced wall thickness (Table 2; Figs. 1c and 1d). Nevertheless, the two designs shared a similar rate of hydrolysis as measured by the accelerated degradation assay (Table 1).

Surgical mortality was 0% and all animals survived until the study end-point (up to 12 months) without anti-platelet or anti-coagulant therapy. Postoperative ultrasound examination revealed that all grafts remained patent, with no incidence of thrombosis or stenosis. Quantification of lumen diameters and qualitative analysis of color Doppler indicated an initial size mismatch between the TEVG and native aorta at 1 month that increased due to an early progressive luminal enlargement (Fig. 2a); this enlargement stabilized by 6 months, however, presumably due to the complete degradation of PGS. Pulse wave and color Doppler imaging demonstrated continuous pulsatile flows, but all grafts created disturbed flows, particularly at the proximal anastomosis, that appeared to be proportional to the degree of graft enlargement (Fig. 2b). It is particularly noteworthy that there was no thrombosis despite disturbed hemodynamics.

Contrast enhanced μCT angiography at 12 months similarly demonstrated a patent graft with free passage of contrast material and no extravasation or filling defect. The graft lumen was adequately size-matched to the native aorta at the anastomotic sites, yet mid-graft luminal enlargement was appreciated, in agreement with ultrasound findings (Fig. 2c).

In contrast to the rapid and widespread cellular infiltration and extensive early remodeling observed in the previously described SCPL PGS–PCL composite grafts,[29] histological observations of the electrospun PGS–PCL grafts showed neotissue formation only on the luminal and abluminal surface of the grafts at 3 months (Fig. 3a). Cellular penetration into the electrospun PGS core was observed at 6 months, with

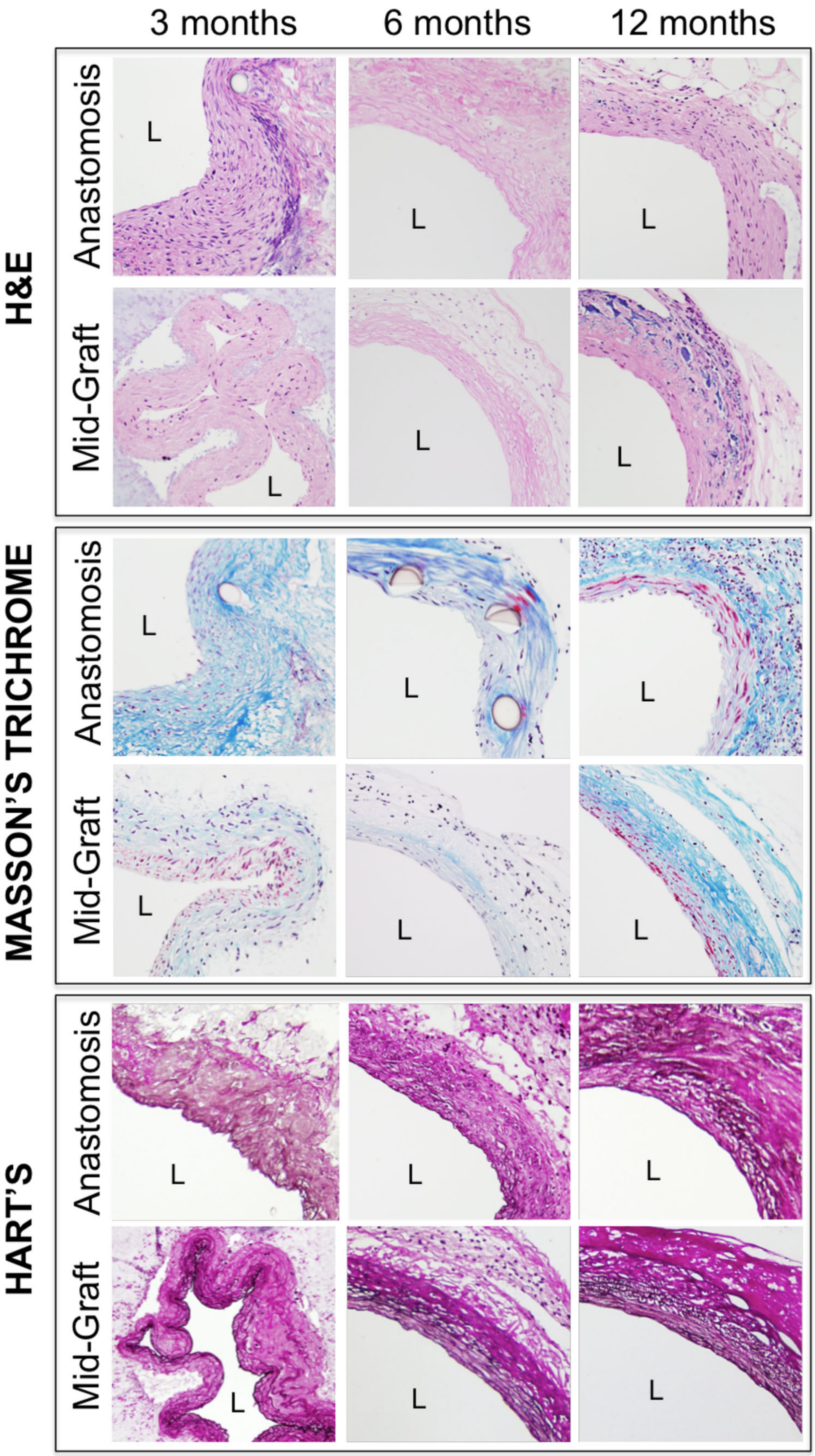
3 months
6 months
12 months
H&E
MASSON'S TRICHROME
HART'S
Anastomosis
Mid-Graft
Anastomosis
Mid-Graft
Anastomosis
Mid-Graft
L

◄**FIGURE 4. Histology of electrospun TEVGs at 3, 6, and 12 months, with representative images of both the anastomosis and the mid-graft (40× magnification). H&E images show luminal tissue formation at 3 months, but limited cellular infiltration prior to 6 months. Masson's Trichrome staining reveals increasing collagen content throughout the implantation period (blue), with significant collagen synthesis at the anastomosis. Hart's stain shows dramatic elastin deposition with lamellar organization as early as 3 months (black) in amounts similar to that present in the adjacent vasculature; this elastin loses its lamellar organization, but otherwise remains essentially unchanged in quantity thereafter. L indicates the lumen.**

nucleated cells detected throughout the thickness of the graft in some regions (Fig. 4). It was also at this time that wall thickness decreased significantly from 455.8 to 160.8 μm, closer to that of the adjacent aorta (118.8 μm) (Fig. 3d). The luminal area of the graft was initially not significantly different from than that of the native aorta, but increased over time, confirming the luminal enlargement observed on ultrasound (Figs. 3a–3c, and 3e). This enlargement was also confirmed by quantifying the luminal circumference from histological images (Fig. 3f). No significant dilatation of TEVG was observed, however, primarily because the PCL sheath did not dilate over the 12 month implantation period (Supplementary Fig. 1).

Staining with Masson's Trichrome revealed substantial collagen accumulation, with increasing collagen content as the graft remodeled over time (Fig. 4). IHC staining confirmed the presence of collagen I and III (data not shown). Hart's staining revealed substantial elastin deposition, with a lamellar organization at 3 months in amounts similar to that of the adjacent vasculature; this elastin lost its lamellar organization at 6 months postimplant, however, and remained essentially unchanged thereafter (Fig. 4).

Calponin and α-SMA staining revealed smooth muscle cells (SMCs) and myofibroblasts in the luminal neotissue at 3 months; a gradual increase in positive staining throughout the graft at 12 months indicated increased cellular infiltration and neotissue formation as the PGS degraded (Fig. 5). Immunofluorescent staining for SM-MHC revealed differentiated, circumferentially organized SMCs in the medial layer of the TEVG as early as 6 months, which persisted to 12 months (Fig. 5). SM-MHC is a late-stage differentiation marker for smooth muscle; strong expression of SM-MHC indicates contractile SMCs.[22]

F4/80 staining demonstrated minimal macrophage infiltration within the graft at 3 and 6 months, but a substantial inflammatory response at 12 months (Fig. 5, Supplementary Fig. 2b). These macrophages appeared to co-localize with regions of residual polymer, suggesting that they actively participate in the degradation or exclusion of the graft at 12 months. Von Kossa staining identified medial calcification associated with remaining scaffold material at 12 months (Supplementary Fig. 2a). The coincidence of late term inflammation and calcification prompted immunofluorescent staining for α-SMA/Cleaved Caspase-3 and α-SMA/RUNX-2; cleaved Caspase-3 is an intracellular marker of apoptosis and RUNX-2 is an osteoblast transcription factor identifying osteogenic progenitors in the TEVG.[17,21,25,26] Osteogenic transdifferentiation and apoptosis of vascular SMCs persisted throughout the 12 month implantation period (Supplementary Fig. 2c–2e).

The electrospun PGS–PCL composite TEVGs exhibited high circumferential structural stiffness throughout remodeling *in vivo*. Pressure-diameter curves demonstrated little compliance in these grafts at 3, 6, and 12 months when compared with the proximal IAA over a pressure range of 10 to 140 mmHg (Fig. 6a). Note that the composite aorta-graft-aorta sample maintained a constant axial force during pressure-diameter testing at the experimentally inferred *in vivo* axial stretch (data not shown). When compared with data at 3 months, there was significant dilatation and structural stiffening of the proximal IAA at 6 months that appeared to be partially reversed at 12 months. In contrast, apart from a decrease in graft thickness (likely secondary to polymer loss), there was little change in the mean structural properties of the grafts throughout the 12-month period of implantation (Fig. 6a), due primarily to the unchanging PCL sheath.

Circumferential Cauchy stress-stretch data suggested that implanted grafts had a significantly higher material stiffness when compared with the proximal IAA, and the material stiffness of the remodeling grafts did not evolve over the 12 months of implantation (Fig. 6b). In contrast, the proximal IAA experienced significant circumferential stiffening from 3 to 6 months, after which it appeared to overcompensate to the presence of a stiff graft by becoming circumferentially more compliant than the native IAA at 12 months. The stiffening of the adjacent IAA from 3 to 6 months may have reflected a remodeling response to compensate for the high stiffness of the interpositional graft. For purposes of comparison, stress–strain curves for SCPL PGS–PCL grafts (adapted from[29]) show that their material stiffness prior to implantation was less than that of the remodeled electrospun PGS–PCL grafts at all times postimplantation (Fig. 6b).

The EDR was used to quantify the deformation-induced strain energy that was lost during cyclic *in vitro* testing due primarily to viscoelastic effects. The

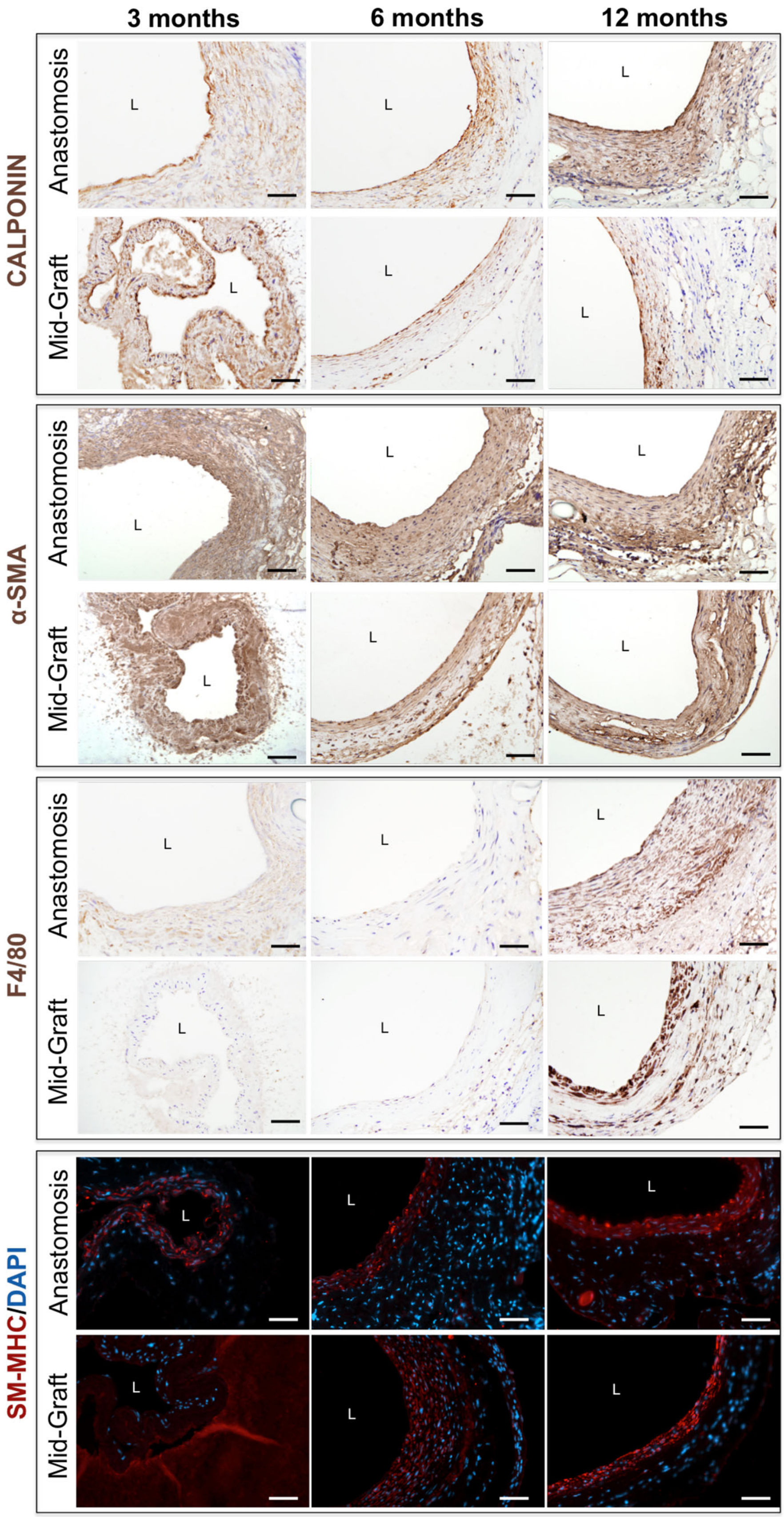
3 months
6 months
12 months
CALPONIN
α-SMA
F4/80
SM-MHC/DAPI
Anastomosis
Mid-Graft
L

◀**FIGURE 5. Immunohistochemical staining of electrospun TEVGs at 3, 6, and 12 months, with representative images of the anastomosis and mid-graft (40× magnification). Calponin and α-SMA staining reveal smooth muscle cells and myofibroblasts only in the luminal neotissue at 3 months, with gradual expansion of positive staining throughout the full thickness of the graft at 12 months indicating increased cellular infiltration and neotissue formation as the PGS degrades. F4/80 staining reveals minimal macrophage infiltration within the graft at 3 and 6 months, but a substantial inflammatory response at 12 months. SM-MHC staining shows differentiated smooth muscle cells in the media-like layer of the TEVG as early as 6 months and persisting to 12 months postimplantation. L indicates the lumen.**

EDR was calculated as the energy difference between loading and unloading curves normalized by the energy associated with loading. It was lower at 3 months, when mostly polymer is present, than that at 12 months, at which time most of the graft consists of neotissue (Supplementary Fig. 3). Although elastin is present, it probably does not contribute functionally to the mechanical properties of the grafts, as suggested by the circumferential stress-stretch data in Fig. 6. Thus, it is the increase in collagen deposition and concurrent degradation of the PGS elastomer resulted in an EDR

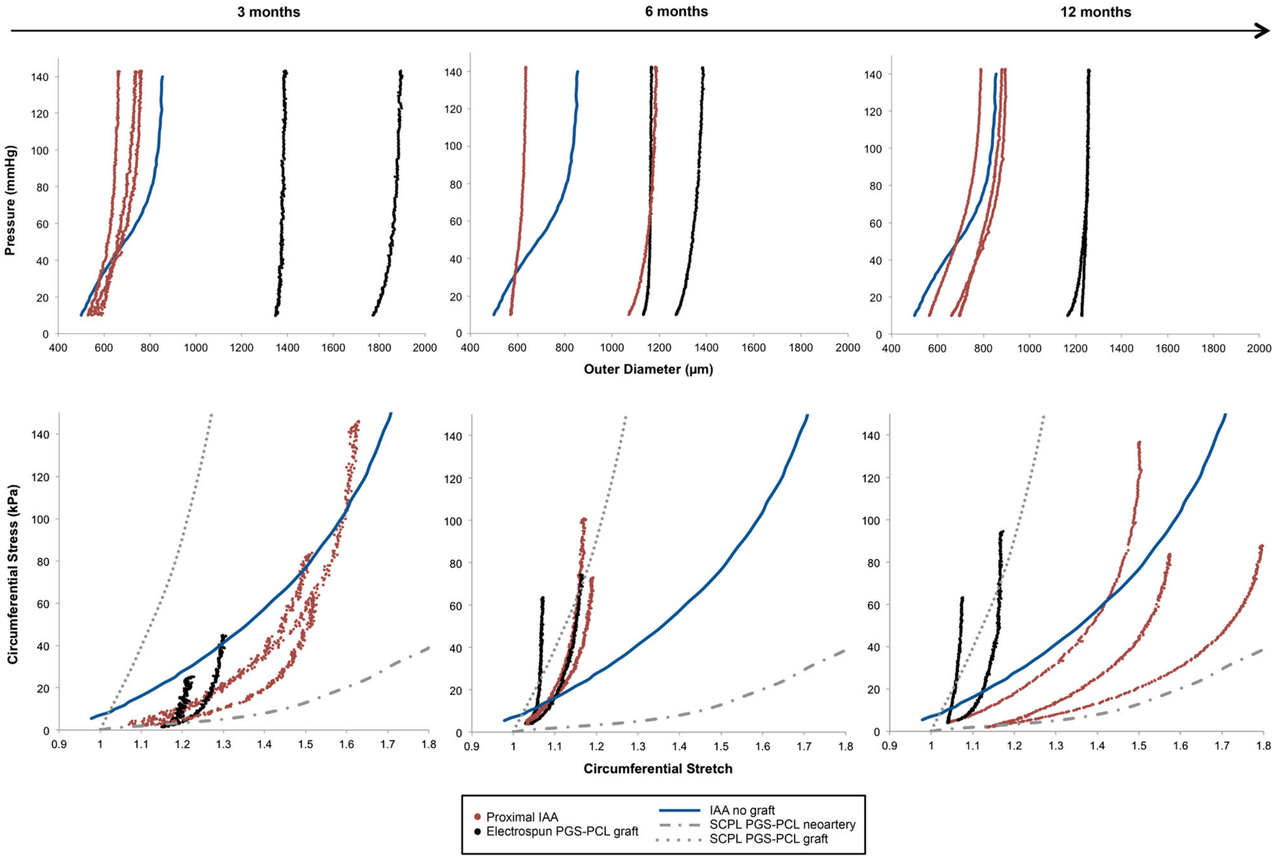

FIGURE 6. (A) Pressure-diameter responses of individual PGS–PCL grafts (shown in black) and adjacent proximal infrarenal abdominal aortas (PIAA) (shown in red) at 3, 6, and 12 months following graft implantation. Data are plotted as the last cycle of unloading at the individual *in vivo* axial stretch following preconditioning. Note the significant mismatch between the outer diameter of the TEVG and the native proximal IAA despite nearly matching the luminal diameters. When compared to findings at 3 months, there is a significant dilation and structural stiffening of the proximal IAA at 6 months that appears to resolve partially by 12 months. In contrast, apart from a decrease in graft thickness (likely secondary to polymer degradation), there is little change in the mean structural properties of the TEVGs throughout the 12-month period of implantation. Also shown for purposes of comparison is the pressure-diameter response for a native proximal IAA in the absence of graft implantation[6] (blue). (B) Circumferential Cauchy stress-stretch data (for individual grafts, shown in black, and adjacent proximal IAAs, shown in red) explanted at 3, 6, and 12 months. Data are plotted as the last cycle of unloading at the individual *in vivo* axial stretch following preconditioning. As can be seen, the grafts have significantly higher material stiffness when compared with the proximal IAA, and this does not appear to evolve throughout the 12 months of implantation. In contrast, the proximal IAA undergoes significant circumferential stiffening from 3 to 6 months, after which it appears to overcompensate by becoming circumferentially more compliant than the native IAA at 12 months. Shown for purposes of comparison are the circumferential Cauchy stress-stretch curve for native IAAs in the absence of a graft[6] (blue) and stress–strain curves adapted from Wu *et al.*[29] for the SCPL PGS–PCL composite grafts both prior to implantation (dotted gray) and after development into neoarteries explanted at 3 months (dashed gray).

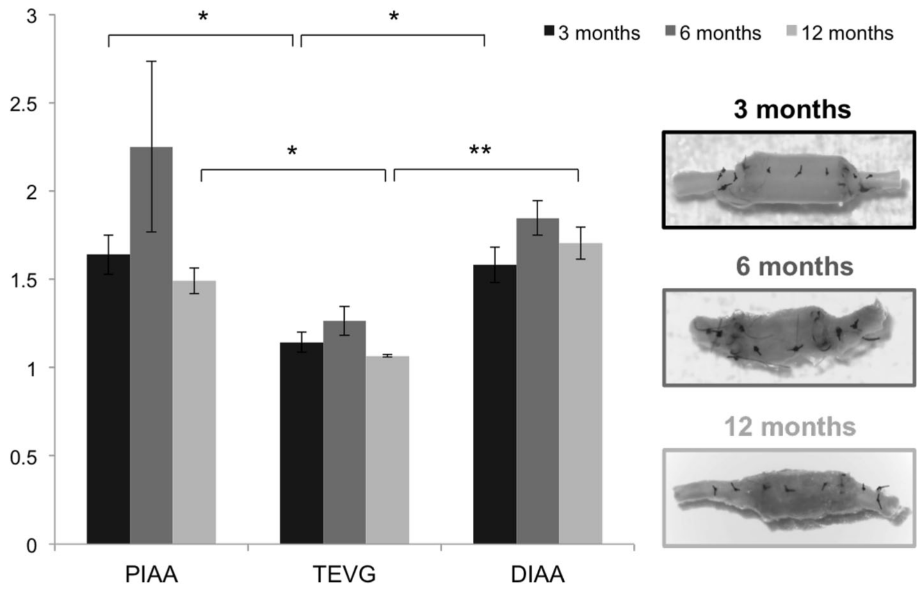

FIGURE 7. Changes in axial retraction upon transection revealed axial remodeling of both the TEVGs and the adjacent proximal and distal infrarenal abdominal aorta (IAA) from 3 to 6 months that partially resolved at 12 months. The *in vivo* axial stretch was calculated as the ratio of the axial distance between suture markers placed on the graft and aorta in the loaded and the unloaded configurations (before and after excision, respectively). The graft was significantly stiffer in the axial direction when compared with the proximal and distal IAA at 3 and 12 months. Also shown are representative images of the excised grafts in the unloaded configuration at the 3 times. As it can be seen, deposition of scar-like collagen at 6 months resulted in buckling at the anastomoses and an associated increased axial retraction upon transection both in the graft and the adjacent aorta. Values are mean ± SEM. * $p<0.05$, ** $p<0.005$.

similar to that of the native IAA in the absence of graft implantation (Supplementary Fig. 3). Perhaps given our limited sample sizes, these differences were not statistically significant.

Changes in retraction upon transection revealed axial remodeling of both the implanted TEVG and the adjacent proximal and distal IAA from 3 to 6 months that partially resolved at 12 months (Fig. 7). The graft was significantly stiffer in the axial direction when compared with the proximal and distal IAA at 3 and 12 months; indeed, it appeared that the deposition of scar-like collagen at 6 months resulted in a buckling at the anastomoses that increased the axial retraction upon transection in both the graft and the adjacent aorta (Fig. 7).

PSR staining suggested that differences in the composition and packing of fibrillar collagens determine the biaxial mechanical properties of both the evolving graft and the remodeled adjacent aorta (Fig. 8a). The relative area fractions of colors, as quantified by PSR colorimetric analysis, revealed a significantly greater proportion of thicker, more densely packed collagen fibers (red and orange) in the adjacent aorta at 6 months (Fig. 8b). These fibers appeared to turnover by 12 months, with the adjacent aorta achieving a fiber distribution and density similar to that at 3 months. In contrast, no such variations in fiber thickness and packing were observed in the luminal or adventitial neotissue deposited within the graft itself. These data are consistent with the observed biaxial mechanical properties of both the graft and the adjacent IAA.

The Hart's stain revealed that elastin formed within the neotissue, yet this elastin did not appear to impact the biaxial mechanical properties of the grafts. The graft contained significant amounts of elastin at 3, 6, and 12 months, with a lamellar organization visible at the earliest time. Quantification of elastin area fractions found no significant difference between the adjacent aorta and the graft itself, and no significant differences in the amount of elastin present at the 3 different explantation times (data not shown). These findings suggest that collagen production and remodeling dominated overall changes in the mechanical properties of the adjacent aorta in response to graft implantation.

DISCUSSION

There are two key differences in physical properties between the current electrospun PGS–PCL murine grafts and the previously fabricated SCPL PGS–PCL rat grafts, both of which were used in an infrarenal

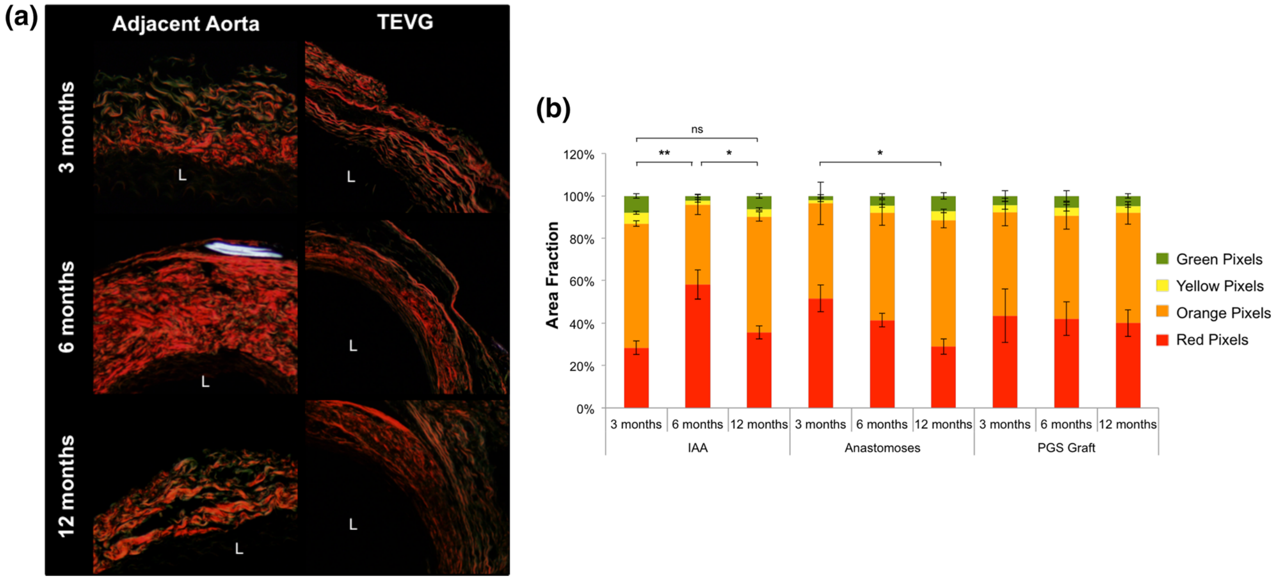

FIGURE 8. Differences in fibrillar collagen composition and packing appear to determine biaxial mechanical properties of the graft and remodeled adjacent aorta. (A) Representative images of Picrosirius Red (PSR) staining (20× magnification) for the adjacent aorta and TEVG at 3, 6, and 12 months. L indicates the lumen. (B) The relative area fraction of collagen fiber birefringence colors, as quantified by PSR colorimetric analysis, revealed a significantly greater proportion of thicker, more densely packed collagen fibers (red and orange) in the adjacent aorta at 6 months. These fibers appeared to turn over by 12 months, with the adjacent aorta achieving a fiber distribution and density similar to that at 3 months. In contrast, no such variation in fiber thickness and packing was observed in the luminal and adventitial neotissue deposited within the graft. These data are consistent with the observed biaxial mechanical behaviors of both the graft and the adjacent IAA presented in Figs. 6a and 6b. Values are mean ± SEM. * $p < 0.05$, ** $p < 0.005$, *ns* indicates not significant.

aortic interposition position.[29] First, the greater initial porosity and larger pore size of the previous graft allowed a more extensive initial cellular infiltration and progressive generation of more space for cellular proliferation and matrix synthesis, resulting in nearly complete host remodeling and integration within 3 months. In contrast, the electrospun PGS–PCL grafts showed reduced porosity, smaller pore diameters, and fiber fusion on the luminal surface, all of which limited the ability of inflammatory cells to infiltrate and initiate the remodeling response. For this reason, although we observed similar cellular composition (differentiated, contractile SMCs) and matrix production (collagen I, III and elastin) in our electrospun grafts as in the SCPL PGS–PCL grafts, this response was significantly delayed, occurring on the order of 6 months and limited to a luminally, rather than interstitially, dominated neotissue formation.

Although pore size was clearly less in the present grafts, precise quantification of the diameters of irregular, ill-defined pores from two-dimensional cross-sections is inherently difficult. We used SEM-based measurement methods because our fibers and pores were smaller than the resolution limit of imaging systems available to us that could produce a 3D-reconstruction. The assumption that the PCL sheath was not porous may have also contributed to a slight overestimation of PGS core porosity; using the opposite assumption of a massless sheath gave a 3% lower average value. Still, given that the low pore diameter and porosity of these grafts is apparent on SEM, the biological relevance of such measurement errors is likely negligible.

Second, there was an initial size mismatch between the electrospun PGS–PCL graft and the murine abdominal aorta that was due to initial limitations in scaling down the physical dimensions of the graft for implantation in a mouse. The thickness of the PGS core was significantly larger than the wall thickness of the murine aorta, and although we had adequate initial matching of luminal diameters, we observed disturbed flow at the proximal anastomosis that appeared to evolve proportional to the progressive luminal enlargement (Fig. 2). This disturbed blood flow may have contributed to the progressive luminal enlargement observed over the first 6 months, especially as it repeatedly localized to the proximal anastomosis. Nevertheless, there was no thrombus and, given the absence of catastrophic failure due to rupture over 12 months, it can be concluded that these grafts have adequate mechanical strength throughout the implantation period.

Of particular importance, pore size appears to be a critical determinant of the overall success of implanted polymeric constructs.[3,8,19,31] If pore size is too small (<10 microns), cells cannot enter the scaffold and they may form a scar plate of collagen, thus encapsulating the construct and increasing the probability of fibrosis or graft failure, as well as associated aberrant remodeling of the adjacent vasculature.[13,27] That is, pore size needs to enable, but also control, cellular infiltration into a degrading scaffold. The current experimental findings were consistent with this expectation: an initial pore size of 1.87 ± 0.23 μm did not allow cellular infiltration, thus explaining why cells were not found in the PGS core at 3 months post-implantation. Furthermore, the small pore size resulted in a chronic inflammation that, coincident with persistent SMC apoptosis and osteogenic transdifferentiation, contributed to late-term TEVG calcification.

Porosity is an important determinant of the relative density and mechanical properties of the initial scaffold, which also influences the hemodynamics.[9] When compared with the SCPL design, the current electrospun grafts exhibited reduced porosity and, consequently, a three-fold higher bulk Young's Modulus. Both methods of fabrication led to a similar rate of accelerated hydrolytic degradation, however. (Note that this degradation assay was not meant to reproduce *in vivo* conditions, but rather to rapidly quantify inherent chemical susceptibility to nucleophilic attack). The presence of organized, differentiated contractile SMCs within the medial region of the TEVG studied herein was likely secondary to the modulus of the PGS core and suggested that the mechanical properties of these electrospun grafts nevertheless promoted vascular cell differentiation despite the late-stage inflammatory response. Given that the initial stiffness of these grafts was on the same order of magnitude as that of the SCPL PGS–PCL grafts, we hypothesize that it was the low porosity, small pore size, and limited pore interconnectivity (not stiffness or hydrolytic degradation rate) that limited extensive interstitial cell infiltration. Clearly, limited cell infiltration reduces the necessary and extensive ECM synthesis required for TEVGs to withstand arterial pressures when the polymer loses load-bearing integrity, at least in the absence of a supporting stiff sheath.

In conclusion, our ultimate goal is to fabricate resorbable cell-free TEVGs that degrade rapidly and promote efficient interstitial neotissue formation while matching the host artery in structural and material properties throughout the course of graft evolution. Such properties would minimize fibrotic responses to foreign materials that prevent efficient integration with host tissues and eliminate adverse remodeling of the adjacent vasculature. The present data not only demonstrate, for the first time, that a very small diameter, electrospun PGS–PCL composite graft is fully functional over 12 months, without thrombus, stenosis, or catastrophic failure, they also provide important qualitative insight and data for informing computational models. Regarding the latter, we previously showed that computational growth and remodeling models can be used to parametrically identify preferred combinations of scaffold properties, both geometric and material, in venous interposition grafts.[15,16] The present data represent the first suitable for informing and developing such a model for bilayered, PGS–PCL TEVGs in the arterial system. If optimized graft parameters can be identified *via* such modeling and realized using electrospinning, or other microfiber fabrication methods, then small diameter rapidly remodeling TEVGs could conceivably be produced in large quantities and at low cost while possessing desirable surgical handling, sufficient compliance, and strength. We submit, therefore, that the improved surgical handling and long-term functional efficacy of this new graft strategy is promising, though results also serve as a cautionary tale—TEVG outcomes will often result from initial scaffold properties, which need to be optimized. Comparison of our present data with prior data suggest that future computational modeling should focus on optimizing initial porosity and pore size of an elastomeric core while identifying a polymeric sheath that sufficiently protects the transformation of the core into neotissue and then degrades.

ELECTRONIC SUPPLEMENTARY MATERIAL

The online version of this article (doi: 10.1007/s10439-015-1545-7) contains supplementary material, which is available to authorized users.

ACKNOWLEDGEMENTS

The Morphology Core at Nationwide Children's Hospital performed histology stainings. The authors are grateful for the expertise of Dr. Kan Hor, Cardiology, Nationwide Children's Hospital, for his assistance with μCT data reconstruction and analysis. This work was supported, in part, by Grants from the NIH: R01 HL128602 (JH, CB, YW), R01 HL089658 (YW), and T32 HL076124 (RK). CB receives Grant support from Gunze Limited and Pall Corporation. The authors have no professional or financial conflicts of interest to disclose.

REFERENCES

[1] Albert, J. D., D. A. Bishop, D. A. Fullerton, D. N. Campbell, and D. R. Clarke. Conduit reconstruction of the right ventricular outflow tract: lessons learned in a twelve-year experience. *J. Thorac. Cardiovasc. Surg.* 106:228–235, 1993.

[2] American Heart Association Statistics Committee and Stroke Statistics Subcommittee. Heart disease and stroke statistics: 2015 update—a report from the American Heart Association. *Circulation* 131:e29–e322, 2015.

[3] Balguid, A., A. Mol, M. H. van Marion, R. A. Bank, C. V. C. Bouten, and F. P. T. Baaijens. Tailoring fiber diameter in electrospun scaffold for optimal cellular infiltration in cardiovascular tissue engineering. *Tissue Eng. Part A* 15:437–444, 2009.

[4] Bersi, M. R., M. J. Collins, E. Wilson, and J. D. Humphrey. Disparate changes in the mechanical properties of murine carotid arteries and aorta in response to chronic infusion of angiotensin-II. *Int. J. Adv. Eng. Sci. Appl. Math.* 4:228–240, 2012.

[5] Dahl, S. L., A. P. Kypson, J. H. Lawson, J. L. Blum, J. T. Strader, Y. Li, R. J. Manson, W. E. Tente, L. DiBernardo, M. T. Hensley, R. Carter, T. P. Williams, H. L. Prichard, M. S. Dey, K. G. Begelman, and L. E. Niklason. Readily available tissue-engineered vascular grafts. *Sci. Transl. Med.* 368:68–69, 2011.

[6] Ferruzzi, J., M. R. Bersi, and J. D. Humphrey. Biomechanical phenotyping of central arteries in health and disease: advantages of and methods for murine models. *Ann. Biomed. Eng.* 41:1311–1330, 2013.

[7] Ferruzzi, J., M. R. Bersi, S. Uman, H. Yanagisawa, and J. D. Humphrey. Decreased elastic energy storage, not increased material stiffness, characterizes central artery dysfunction in Fibulin-5 deficiency independent of sex. *J. Biomech. Eng.* 137:031007, 2015.

[8] Garg, K., N. A. Pullen, C. A. Ozkeritzian, J. J. Ryan, and G. L. Bowlin. Macrophage functional polarization (M1/M2) in response to varying fiber and pore dimensions of electrospun scaffolds. *Biomaterials* 34:4439–4451, 2013.

[9] Gibson, L. J., and M. F. Ashby. Cellular Solids: Structure and Properties. Oxford: Pergamon Press, 1988.

[10] Gleason, R. L., S. P. Gray, E. Wilson, and J. D. Humphrey. A multiaxial computer-controlled organ culture and biomechanical device for mouse carotid arteries. *ASME J. Biomech. Eng.* 126:787–795, 2004.

[11] Hibino, N., E. McGillicuddy, G. Matsumura, Y. Ichihara, Y. Naito, C. Breuer, and T. Shinoka. Late-term results of tissue-engineered vascular grafts in humans. *J. Thorac. Cardiovasc. Surg.* 139:431–436, 2010.

[12] Jeffries, E. M., R. A. Allen, J. Gao, M. Pesce, and Y. Wang. Highly elastic and suturable electrospun poly(glycerol sebacate) fibrous scaffolds. *Acta Biomater.* 18:30–39, 2015.

[13] Junge, K., M. Binnebosel, K. T. vonTrotha, R. Rosch, U. Klinge, U. P. Neumann, and P. Lynen Jansen. Mesh biocompatibility: effects of cellular inflammation and tissue remodeling. *Langenbecks Arch. Surg.* 397:255–270, 2012.

[14] Lopez-Soler, R. I., M. P. Brennan, A. Goyal, Y. Wang, P. Fong, G. Tellides, A. Sinusas, A. Dardik, and C. K. Breuer. Development of a mouse model for evaluation of small diameter vascular grafts. *J. Surg. Res.* 139:1–6, 2007.

[15] Miller, K. S., R. Khosravi, C. K. Breuer, and J. D. Humphrey. Hypothesis-driven parametric study to demonstrate the predictive capability of a computational model of in vivo neovessel development and the role of construct physical properties. *Acta Biomater.* 11:283–294, 2015.

[16] Miller, K. S., Y. U. Lee, Y. Naito, C. K. Breuer, and J. D. Humphrey. Computational model of in vivo neovessel development from an engineered polymeric vascular construct. *J. Biomech.* 47:2080–2087, 2014.

[17] New, S. E. P., and E. Aikawa. Cardiovascular calcification. *Circ. J.* 75:1305–1313, 2011.

[18] Niklason, L. E., J. Gao, W. M. Abbott, K. K. Hirschi, S. Houser, R. Marini, and R. Langer. Functional arteries grown in vitro. *Science* 284:489–493, 1999.

[19] Pham, Q. P., U. Sharma, and A. G. Mikos. Electrospun poly(CL) microfiber and multilayer nanofiber/microfiber scaffolds: characterization of scaffolds and measurement of cellular infiltration. *Biomacromolecules* 7:2796–2805, 2006.

[20] Pomerantseva, I., N. Krebs, A. Hart, C. M. Neville, A. Y. Huang, and C. A. Sundback. Degradation behavior of poly(glycerol sebacate). *J. Biomed. Mater. Res. A.* 91:1038–1047, 2009.

[21] Raggi, P. Inflammation and calcification: the chicken or the hen? *Atherosclerosis* 238:173–174, 2015.

[22] Rensen, S. S. M., P. A. F. M. Doevendans, and G. J. J. M. van Eys. Regulation and characteristics of vascular smooth muscle cell phenotypic diversity. *Neth. Heart J.* 15:100–108, 2007.

[23] Roh, J. D., G. N. Nelson, M. P. Brennan, T. L. Mirensky, T. Yi, T. Hazlett, G. Tellides, A. J. Sinusas, J. S. Pober, W. M. Saltzman, T. R. Kyriakides, and C. K. Breuer. Small-diameter biodegradable scaffolds for functional vascular tissue engineering in the mouse model. *Biomaterials* 29:1454–1463, 2008.

[24] Seifu, D. G., A. Purnama, K. Mequanint, and D. Mantovani. Small-diameter vascular tissue engineering. *Nat. Rev. Cardiol.* 10:410–421, 2013.

[25] Shanahan, C. M. Inflammation ushers in calcification: a cycle of damage and protection? *Circulation.* 116:2782–2785, 2007.

[26] Tara, S., H. Kurobe, K. A. Rocco, M. W. Maxfield, C. A. Best, T. Yi, Y. Naito, C. K. Breuer, and T. Shinoka. Well-organized neointima of large-pore poly(L-lactic acid) vascular graft coated with poly(L-lactic-co-ε-caprolactone) prevents calcific deposition compared to small-pore electrospun poly(L-lactic acid) graft in a mouse aortic implantation model. *Atherosclerosis* 237:684–691, 2014.

[27] Udelsman, B. V., R. Khosravi, K. S. Miller, E. W. Dean, M. R. Bersi, K. Rocco, T. Yi, J. D. Humphrey, and C. K. Breuer. Characterization of evolving biomechanical properties of tissue engineered vascular grafts in the arterial circulation. *J. Biomech.* 47:2070–2079, 2014.

[28] Wang, Y., G. A. Ameer, B. J. Sheppard, and R. Langer. A tough biodegradable elastomer. *Nat. Biotechnol.* 20:602–606, 2002.

[29] Wu, W., R. A. Allen, and Y. Wang. Fast-degrading elastomer enables rapid remodeling of a cell-free synthetic graft into a neoartery. *Nat. Med.* 18:1148–1153, 2012.

[30] Wystrychowski, W., T. N. McAllister, K. Zagalski, N. Dusserre, L. Cierpka, and N. L'Heureux. First human use of an allogeneic tissue-engineered vascular graft for hemodialysis access. *J. Vasc. Surg.* 60:1353–1357, 2014.

[31] Zander, N. E., J. A. Orlicki, A. M. Rawlett, and T. P. Beebe. Electrospun polycaprolactone scaffolds with tailored porosity using two approaches for enhanced cellular infiltration. *J. Mater. Sci. Mater. Med.* 24:179–187, 2013.